CrystEngComm

Dynamic Structural Reconstruction of (Guanidinium^{+})$_2$(Benzene-1,4-disulfonate^{2-}) Host Crystal by Guest Adsorption

Journal:	*CrystEngComm*
Manuscript ID	CE-ART-11-2020-001616.R1
Article Type:	Paper
Date Submitted by the Author:	05-Dec-2020

Complete List of Authors:	Abe, Haruka; Tohoku University, Sendai 980-8579, Japan., Graduate School of Engineering Kobayashi, Takahiro; Tohoku University, Sendai 980-8579, Japan., Graduate School of Engineering Hoshino, Norihisa; Tohoku University Graduate School of Engineering School of Engineering, IMRAM, Tohoku Univ. Takeda, Takashi; Tohoku University, Institute of Multidisciplinary Research for Advanced Materials Suzuki, Yasutaka; Yamaguchi University, Graduate School of Medicine Kawamata, Jun; Yamaguchi University, Graduate School of Medicine Akutagawa, Tomoyuki; Tohoku University, Institute of Multidisciplinary Research for Advanced Materials

ARTICLE

Dynamic Structural Reconstruction of (Guanidinium^{+})$_2$(Benzene-1,4-disulfonate^{2-}) Host Crystal by Guest Adsorption

Haruka Abe,[a] Takahiro Kobayashi,[a] Norihisa Hoshino,[a, b] Takashi Takeda,[a, b] Yasutaka Suzuki,[c] Jun Kawamata,[c] and Tomoyuki Akutagawa[a, b]*

Received 00th January 20xx,
Accepted 00th January 20xx

DOI: 10.1039/x0xx00000x

Guanidinium (**G**$^{+}$) and benzene-1,4-disulfonate (**BDS**$^{2-}$) form a rigid electrostatic cation–anion crystal lattice, which undergoes an interesting dynamic structural reconstruction through guest adsorption–desorption processes with H_2O, pyrrole (Pyrr), pyrazine (Pyz), thiophene (TP), pyridine (Py), 1,4-dioxane (Diox), or aniline (Ani). The host lattice of bis(guanidinium) benzene-1,4-disulfonate, (**G**$^{+}$)$_2$(**BDS**$^{2-}$), which does not contain void spaces initially, changed to host–guest crystals of (**G**$^{+}$)$_2$(**BDS**$^{2-}$)•(Guest)$_x$ upon guest adsorption (x = 1, 2, and 3). The cation–anion electrostatic N–H^{+}•••$^{-}$O$_3$S– hydrogen bonds between the **G**$^{+}$ cation and **BDS**$^{2-}$ dianion formed tightly bound two-dimensional (2D) structures. These layers are connected by perpendicular **BDS**$^{2-}$ dianions, forming the guest adsorption crystalline pores. The adsorption–desorption isotherm for Diox at 298 K indicated the formation of (**G**$^{+}$)$_2$(**BDS**$^{2-}$)•(Diox)$_3$, which was consistent with the single-crystal X-ray structural analysis. Single crystals of (**G**$^{+}$)$_2$(**BDS**$^{2-}$)•(Py-H_2O)$_2$ consist of two hydrogen-bonded [(**G**$^{+}$)$_2$(**BDS**$^{2-}$)]$_2$ bilayers connected by the **BDS**$^{2-}$ dianions, forming crystalline pores that accommodate 2 Py guest molecules. The H_2O molecules in (**G**$^{+}$)$_2$(**BDS**$^{2-}$)•(Py-H_2O)$_2$ are lodged in the intralayer, leading to the [(**G**$^{+}$)$_2$(**BDS**$^{2-}$)•••(H_2O)$_2$•••(**G**$^{+}$)$_2$(**BDS**$^{2-}$)] hydrogen-bonded bilayer. The electrostatic cation–anion host lattice of (**G**$^{+}$)$_2$(**BDS**$^{2-}$) responded to the guest adsorption–desorption cycle by a dynamic structural reconstruction. A guest adsorption of polar Ani into (**G**$^{+}$)$_2$(**BDS**$^{2-}$) host changed the crystal symmetry from centric *P*-1 to acentric *P*2$_1$ of (**G**$^{+}$)$_2$(**BDS**$^{2-}$)•(Ani)$_3$.

Introduction

The formation of highly designable molecular assemblies is enabled by various intermolecular forces such as electrostatic, hydrogen bonding, charge-transfer, dipole-dipole, hydrophobic, and van der Waals interactions. The energies of these interactions range from 0.1–2 kJ mol^{-1} (van der Waals) and 5–20 kJ mol^{-1} (hydrogen bonding) to approximately 100 kJ mol^{-1} (electrostatic interactions).[1–4] Among the intermolecular forces, the electrostatic cation–anion interaction is an interesting approach to form thermally stable, structurally rigid, and dynamic molecular assemblies in ionic liquids.[5] Electrostatic supramolecular assemblies based on ionic liquid[6,7] and molecular crystals[8–13] have been employed in functional π-molecular systems such as high-temperature ferroelectrics,[9–12] organic semiconductors,[12,13] hierarchical nanostructured materials,[14,15] and optically active cation–anion receptors.[16,17] Among the electrostatically bound supramolecular assemblies, cation–anion salt-based dynamic host–guest crystal lattices are interesting research targets in the design of highly stable host crystal lattices.[18–20] Highly stable host lattices in metal organic frameworks (MOFs) and covalent organic frameworks (COFs) with strong coordination and covalent bonds (>100 kJ mol^{-1}) enabled the fabrication of rigid molecular assemblies.[21–24] In contrast, hydrogen bonded organic frameworks (HOFs) have recently attracted much attention as flexible and renewable resources for the fabrication of selective guest adsorption materials,[25–33] and feature intermolecular hydrogen bonds in the range of 5–20 kJ mol^{-1}.[34-36] An essential prerequisite for the use of intermolecular hydrogen bonds is the design of molecules in which the directionality and strength of the intermolecular interactions can be controlled, thus enabling the construction of various crystalline spaces for the capture of specific guest molecules by the pore spaces of the HOF. Simple spherical cations and anions, such as metal and halide ions, render the design of anisotropic intermolecular interactions difficult because of the formation of closest-packing structures. However, highly designable organic cations and anions are useful building blocks for various dynamic host–guest frameworks because of the electrostatic intermolecular interactions that maintain the rigid host framework through the guest adsorption–desorption cycle. The energy of electrostatic interactions, which lie between those of coordination and hydrogen bonds, enables the preparation of dynamic and flexible host frameworks for the guest adsorption–desorption cycle.

[a] *Graduate School of Engineering, Tohoku University, Sendai 980-8579, Japan.*
[b] *Institute of Multidisciplinary Research for Advanced Materials (IMRAM), Tohoku University, 2-1-1 Katahira, Aoba-ku, Sendai 980-8577, Japan*
[c] *Graduate School of Sciences and Technology for Innovation, Yamaguchi University, 1677-1 Yoshida, Yamaguchi 753-8512, Japan*

Electronic Supplementary Information (ESI) available: TG charts of (**G**$^{+}$)$_2$(**BDS**$^{2-}$)•(Guest)$_x$ crystals, crystal structures of (**G**$^{+}$)$_2$(**BDS**$^{2-}$)•(THF)$_2$, hydrogen-bonded bilayer of (**G**$^{+}$)•••(H_2O)•••(**G**$^{+}$), crystal structures of (**G**$^{+}$)$_2$(**BDS**$^{2-}$)•(Benzene)$_3$, (**G**$^{+}$)$_2$(**BDS**$^{2-}$)•(TP)$_3$, (**G**$^{+}$)$_2$(**BDS**$^{2-}$)•(Pyrr)$_3$, and (**G**$^{+}$)$_2$(**BDS**$^{2-}$)•(Ani)$_3$, polar Ani arrangement in the *ac* plane, temperature and time dependent PXRD changes of (**G**$^{+}$)$_2$(**BDS**$^{2-}$)•(THF)$_2$. See DOI: 10.1039/x0xx00000x

The three-fold symmetrical guanidine molecule can accept a proton (H^+) to form the guanidinium (**G**$^+$) cation, which engages in hydrogen bonding. Upon mixing guanidine with a sulfonic acid derivative (*R*-SO_3H), intermolecular proton transfer delivers the cation–anion ion-paired salt (**G**$^+$)(*R*–SO_3^-). Subsequently, a network of intermolecular hydrogen bonds N–H^+•••^-O_3S–*R* forms a two-dimensional (2D) structure.[37–42] By designing the *R*-group in the sulfonate anion, a variety of interesting molecular assemblies with physical functionalities can be obtained. For example, the simple inorganic (**G**$^+$)(Al^{3+})(SO_4^{2-})$_2$ salt is a well-known ferroelectric material,[43] whereas the organic sulfate (**G**$^+$)(C_2H_5O-SO_3^-) salt shows a ferroelectric polarization–electric field (*P*–*E*) hysteresis curve at 170 K.[44] The temperature-dependent order–disorder conformational change of the C_2H_5O– group in the 2D-electrostatic layer is indicated by the ferroelectric–paraelectric phase transition at 210 K, and the collective motion of the flexible C_2H_5O– groups plays an important role in the dipole inversion and ferroelectricity. Design of the *R*-unit can form interesting soft materials. For example, the formation of a smectic liquid crystalline phase in (**G**$^+$)($C_nH_{2n+1}SO_3^-$) with n=6–18 is related to the thermally activated molecular motion of alkyl chains on the electrostatic hydrogen-bonded rigid layer, where the sliding motion of each layer appeared as a mesophase.[45] The crystal structures of the hydrogen-bonded supramolecules (**G**$^+$)(*p*-X-$C_4H_4SO_3^-$) with X=–CH_3, –NH_2, –OCH_3, –NO_2, –OH, and –COOH have been designed to form non-linear optical materials, and the para-substituent (X) on the aromatic ring affected the crystal symmetry and second-harmonic generation (SHG) activity.[46] Among a variety of **G**$^+$ – organosulfonates crystals, a simple hydrogen-bonding molecular assembly between **G**$^+$ and benzene-1,4-disulfonate (**BDS**$^{2-}$) is a prototype of the fabrication for new host–guest compounds of (**G**$^+$)$_2$(**BDS**$^{2-}$)•(Guest)$_x$. For instance, the guest inclusion pillar array has been observed in single-crystals of (**G**$^+$)$_2$(**BDS**$^{2-}$)•(Benzene)$_3$,[47] and the expansion of the pillar unit from benzene to naphthalene or anthracene can include the guest molecules of naphthalene and anthracene.[48] Tightly interacted (**G**$^+$)$_2$(**BDS**$^{2-}$) unit without the pore can reconstruct the crystal structures according to the size and shape of the guest molecules. Recently, it has been reported that the single-crystals of (**G**$^+$)$_2$(**BDS**$^{2-}$)•(Acetone)$_2$ show interesting single-crystals-to-single-crystal transformation to form (**G**$^+$)$_2$(**BDS**$^{2-}$) bearing pillared pores.[49] Further chemical designs by Ward et al., enables to show the single-crystal-to-single-crystal transformation using new dianions of 1,2,4,5-tetra(4-sulfonatophenyl)benzene (TSPB) or 1,3,5-tri(4-sulfophenyl)benzene, where the crystal structures of guest desorption state have been clearly solved in the single-crystal X-ray structural analyses.[50,51] From the viewpoint of physical properties of these host–guest crystals, the 2D molecular crystals of (**G**$^+$)$_2$(4,4'-biphenyldisufonate^{2-}) and (**G**$^+$)$_2$(1,5-napthalenedisufonate^{2-}) showed high proton conductivities of 0.75×10^{-2} S cm^{-1} and 1.8×10^{-2} S cm^{-1} under humidified conditions at 300 K, respectively, and their crystal structures consist of pillared biphenyl and naphthalene units perpendicular to the 2D N–H^+•••^-O_3S– hydrogen-bonded layers.[52] In addition, the 2D-pillared supramolecule (**G**$^+$)$_2$(4,4'-biphenyldisufonate^{2-}) can form various host–guest crystals with benzene derivatives such as 1,4-dichlorobenzene, *o*-xylene, 1,4-divinylbenzene, and nitrobenzene, and has been utilised as a crystal sponge for the structure determination of the guest molecules.[53] The electrostatically bound (**G**$^+$)(*R*-SO_3^-) supramolecular assemblies are interesting structural building blocks for dynamic host–guest crystalline materials. Herein, we report the structural reconstruction from guest-free to host–guest supramolecular assemblies (**G**$^+$)$_2$(**BDS**$^{2-}$)•(Guest)$_x$ (x = 1, 2, and 3), where **BDS**$^{2-}$ is benzene-1,4-disulfonate and Guest is H_2O, pyrrole (Pyrr), pyrazine (Pyz), thiophene (TP), pyridine (Py), tetrahydrofuran (THF), benzene (Benz), 1,4-dioxane (Diox), or aniline (Ani) (Scheme 1). The crystal structures of (**G**$^+$)$_2$(**BDS**$^{2-}$)•(THF)$_2$ and (**G**$^+$)$_2$(**BDS**$^{2-}$)•(Benz)$_3$ have been already reported by Ward et al., and the THF adsorption – desorption isotherm of (**G**$^+$)$_2$(**BDS**$^{2-}$)•(THF)$_2$ crystals is evaluated to clarify the guest inclusion behaviours.[37-39] The Connolly solvent excluded volume of guest molecule (V_G) increased in the order of H_2O (10 Å^3), Pyrr (56 Å^3), Pyz (60 Å^3) ~ TP (61 Å^3), Py (65 Å^3), THF (71 Å^3) ~ Benz (71 Å^3), Diox (78 Å^3), to Ani (80 Å^3),[54] which were occupied in the void space of electrostatic (**G**$^+$)$_2$(**BDS**$^{2-}$) lattice after the guest adsorption. The crystal structure of guest-free (**G**$^+$)$_2$(**BDS**$^{2-}$) features charge supported hydrogen bonds without guest adsorption pores. While the crystal structures of (**G**$^+$)$_2$(**BDS**$^{2-}$)•(Guest)$_x$ depended on the guest molecules, a hydrogen-bonded simple brick of [(**G**$^+$)$_2$(**BDS**$^{2-}$)] and bilayer of [(**G**$^+$)$_2$(**BDS**$^{2-}$)]$_2$ were observed in (**G**$^+$)$_2$(**BDS**$^{2-}$)•(Benz, Diox, Ani, Pyrr, or TP)$_3$ and (**G**$^+$)$_2$(**BDS**$^{2-}$)•(H_2O, Pyz, THF or Py-H_2O)$_2$, respectively. The dynamic structural reconstruction that accompanies the pillar stacking process of the **BDS**$^{2-}$ dianion within the 2D electrostatic hydrogen-bonded layer was triggered by the guest molecule adsorption–desorption processes.

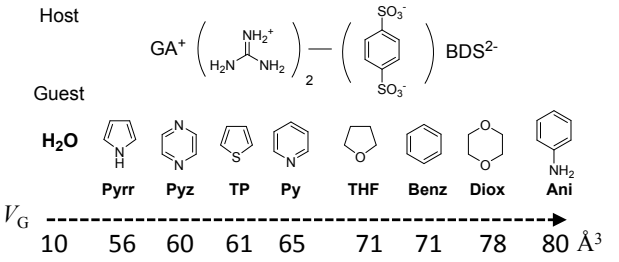

Scheme 1. Molecular structures of the (**G**$^+$)$_2$(**BDS**$^{2-}$) dynamic host framework and guest molecules H_2O, pyrrole (Pyrr), pyrazine (Pyz), thiophene (TP), pyridine (Py), tetrahydrofuran (THF), benzene (Benz), 1,4-dioxane (Diox), or aniline (Ani).

Experimental

General. Commercially available reagents and solvents were used without further purification. Infrared spectra (IR, 400–4000 cm^{-1}) were measured using KBr pellets on a Thermo Fisher Scientific Nicolet 6700 spectrophotometer with a resolution of 4 cm^{-1}. Thermogravimetric (TG) analyses were conducted using a Rigaku Thermo plus TG8120 thermal analysis station with an Al_2O_3 reference at a heating and cooling rates of 5 K min^{-1} under nitrogen. The adsorption and desorption isotherms for Diox at

298 K and THF at 283 K were measured with a BELSORP-aqua automatic volumetric adsorption apparatus (BEL Japan, Inc.). The $(\mathbf{G}^+)_2(\mathbf{BDS}^{2-})$ crystalline powder was heated under reduced pressure (373 K, $<10^{-2}$ Pa) to remove the surface-bound H_2O molecules prior to analysis.

Preparation of host–guest molecular crystals. Single crystals of $(\mathbf{G}^+)_2(\mathbf{BDS}^{2-})$ were obtained by mixing guanidinium carbonate $(\mathbf{G}^+)_2CO_3^{2-}$ (361 mg, 2.01 mmol) and benzene-1,4-disulfonic acid (552 mg, 2.32 mmol) in H_2O (1 mL).[42] The colourless powder was recrystallized from boiling H_2O (1 mL), and the obtained colourless platelets were collected by filtration. Elemental analysis of $(\mathbf{G}^+)_2(\mathbf{BDS}^{2-})$. Calcd. for $C_8H_{16}N_6O_6S_2$: C, 26.96; H, 4.53; N, 23.58. Found: C, 26.88; H, 4.48; N, 23.33. The host–guest molecular crystals of $(\mathbf{G}^+)_2(\mathbf{BDS}^{2-})$•(Benz, Diox, Ani, TP, or Pyrr)$_3$, $(\mathbf{G}^+)_2(\mathbf{BDS}^{2-})$•(THF or Py-$H_2O$)$_2$, and $(\mathbf{G}^+)_2(\mathbf{BDS}^{2-})$•($H_2O$) were obtained by recrystallization of $(\mathbf{G}^+)_2(\mathbf{BDS}^{2-})$ from benzene/CH_3OH (v/v = 1:1), 1,4-dioxane/H_2O (v/v = 1:1), aniline/CH_3OH (v/v = 2:3), thiophene/CH_3OH (v/v = 1:4), pyrrole/CH_3OH (v/v = 2:1), THF/H_2O (v/v = 3:2), pyridine/H_2O (v/v = 1:1), and toluene/CH_3OH (v/v = 1:2) mixtures, respectively. Single crystals of $(\mathbf{G}^+)_2(\mathbf{BDS}^{2-})$•(Pyz) was obtained by recrystallization of $(\mathbf{G}^+)_2(\mathbf{BDS}^{2-})$ from CH_3OH under the excess amount of Pyz.

Table 1. Crystallographic data and data collection and reduction parameters of $(G^+)_2(BDS^{2-})$ (**1**) and **1**•(Guest) crystals.

Crystal	**1**	**1**•(H_2O)	**1**•(Pyz)	**1**•(Py-H_2O)$_2$
Chemical formula	$C_8H_{16}N_6O_6S_2$	$C_8H_{18}N_6O_7S_2$	$C_{12}H_{20}N_8O_6S_2$	$C_{18}H_{30}N_8O_8S_2$
Formula weight	356.37	374.39	436.46	550.60
T, K	100	100	100	100
Space group	*P*-1 (#2)	*Pnma* (#62)	$P2_1/c$ (#14)	$P2_1/c$ (#14)
a, Å	6.73165(19)	21.3840(6)	5.94009(17)	10.3886(2)
b, Å	7.0727(2)	8.2026(2)	7.4700(2)	7.34813(19)
c, Å	7.95197(18)	8.2026(2)	20.0860(6)	17.1099(3)
α, degrees	86.2104(17)	–	–	–
β, degrees	72.5954(18)	–	90.581(6)	103.338 (1)
γ, degrees	85.649(2)	–	–	–
V, Å^3	359.851(17)	1684.60(8)	891.22(4)	1270.88(5)
Z	1	4	2	2
D_{calc}, g·cm^{-3}	1.644	1.476	1.626	1.439
μ, cm^{-1}	37.611	32.865	31.963	24.235
Refs. meas.	4160	17983	9589	13862
Indep. Refs.	1299	1654	1621	2329
Refs.used	1299	1654	1621	2329
R_{int}	0.0419	0.0634	0.0662	0.0317
R_1 [a]	0.0357	0.0975	0.0535	0.0366
R_{all}	0.0382	0.1194	0.0575	0.0414
$R_w(F_2)$ [a]	0.0996	0.2930	0.1606	0.1024
Max res., e$^-$Å^{-3}	0.33	1.10	0.46	0.50
Min res., e$^-$Å^{-3}	−0.41	−0.90	−0.59	−0.45
GOF	1.119	1.238	1.074	1.110
CCDC	1997034	2041223	2041222	1997210

[a] $R_1=\Sigma||F_o|-|F_c||\,/\,\Sigma\,|F_o|$ and $R_w=(\Sigma\omega(|F_o|-|F_c|)2\,/\,\Sigma\omega F_o^2)^{1/2}$.

Crystal	**1**•(Ani)$_3$	**1**•(Diox)$_3$	**1**•(TP)$_3$	**1**•(Pyrr)$_3$
Chemical formula	$C_{26}H_{37}N_9O_6S_2$	$C_{20}H_{40}N_6O_{12}S_2$	$C_{20}H_{28}N_6O_6S_5$	$C_{20}H_{31}N_9O_6S_2$
Formula weight	635.76	620.69	608.78	557.65
T, K	100	100	100	100
Space group	$P2_1$ (#4)	$P2_1/n$ (#14)	$P2_1/n$ (#14)	$P2_1/n$ (#14)
a, Å	7.5488(2)	7.6145(3)	7.6230(4)	7.4854(5)
b, Å	18.0321(6)	12.3230(5)	16.8745(8)	12.0766(7)
c, Å	11.5759(4)	15.6653(5)	11.8090(6)	16.8284(10)
α, degrees	–	–	–	
β, degrees	91.052(6)	101.077(2)	90.488(6)	90.093(6)
γ, degrees	–	–	–	
V, Å^3	1575.45(9)	1442.53(9)	1518.98(12)	1521.25(16)
Z	2	2	2	2
D_{calc}, g·cm^{-3}	1.340	1.429	1.453	1.211
μ, cm^{-1}	19.913	22.825	22.576	19.906
Refs. meas.	17391	15727	16884	16695
Indep. Refs.	5566	2638	2751	2776
Refs.used	5566	2638	2751	2776
R_{int}	0.0447	0.0849	0.0531	0.0796
R_1 [a]	0.0395	0.0581	0.0950	0.1099
R_{all}	0.0578	0.0735	0.1118	0.1770
Max res., e$^-$Å^{-3}	0.23	0.39	0.00	0.00
Min res., e$^-$Å^{-3}	−0.34	−0.56	−0.00	−0.00
$R_w(F_2)$ [a]	0.0991	0.1536	0.3084	0.3472
GOF	1.036	1.009	1.083	1.901
CCDC	2041224	1997035	2041225	2041226

[a] $R_1=\Sigma||F_o|-|F_c||\,/\,\Sigma\,|F_o|$ and $R_w=(\Sigma\omega(|F_o|-|F_c|)2\,/\,\Sigma\omega F_o^2)^{1/2}$.

Crystal structure determination. Single crystals were obtained by the slow evaporation method. Temperature-dependent crystallographic data (Table 1) were collected using a Rigaku RAPID-II diffractometer equipped with a rotating anode fitted with a multilayer confocal optic, using Cu Kα (λ=1.54187 Å) radiation from a graphite monochromator. Structural refinements were performed using the full-matrix least-squares method on F^2. Calculations were performed using Crystal Structure software packages.[55,56] All parameters were refined using anisotropic temperature factors, except for those of the hydrogen atoms. The guest molecules of single-crystals $(\mathbf{G}^+)_2(\mathbf{BDS}^{2-})$•(guest)$_3$ indicated a rapid desorption at 298 K during the crystal mount on capillary, which decreased the quality of the structural analyses. The disordered Py and TP guest molecules in single-crystals of $(\mathbf{G}^+)_2(\mathbf{BDS}^{2-})$•(Py)$_3$ $(\mathbf{G}^+)_2(\mathbf{BDS}^{2-})$•(TP)$_3$ were removed from the structural refinements after a SQUEEZE procedure. The hydrogen atoms of disordered molecules were removed in the structural refinements. Temperature-dependent powder X-ray diffraction (PXRD) was performed using a Rigaku SmartLab diffractometer with Cu Kα (λ=1.54187 Å) radiation.

Results and Discussion

Formation of $(G^+)_2(BDS^{2-})\bullet(Guest)_x$ crystals.

The high thermal stability of the guest-free $(G^+)_2(BDS^{2-})$ crystals (thermal decomposition temperature: 580 K) is due to the electrostatic intermolecular interactions between the cationic G^+ and the dianionic BDS^{2-}. Recrystallisation of $(G^+)_2(BDS^{2-})$ in the existence of Diox, Ani, TP, Pyrr, Py, Pyz, or toluene, led to formation of single crystals of composition $(G^+)_2(BDS^{2-})\bullet$(Diox, Ani, TP, or Pyrr)$_3$, $(G^+)_2(BDS^{2-})\bullet$(Py-H_2O)$_2$, and $(G^+)_2(BDS^{2-})\bullet$(Pyz or H_2O) as revealed by single-crystal X-ray structural analyses at 100 K. The crystal formula of single crystals $(G^+)_2(BDS^{2-})$:(Guest) were observed at 1:3, 1:2, and 1:1, according to the guest molecules. Instead of the formation of $(G^+)_2(BDS^{2-})\bullet$(Toluene)$_3$, single crystals of $(G^+)_2(BDS^{2-})\bullet(H_2O)$ were obtained by the recrystallisation of CH_3OH/toluene mixed solvent. The TG measurements of the host–guest crystals indicated that the loss of the guest molecules occurred at approximately 300 K (Fig. S1), suggesting that the guest-containing $(G^+)_2(BDS^{2-})$ crystal lattice becomes unstable because of thermally activated motions.

Crystal structure of guest-free $(G^+)_2(BDS^{2-})$.

Fig. 1 presents the crystal structure of guest-free $(G^+)_2(BDS^{2-})$. One G^+ cation and a half unit of BDS^{2-} dianion are the crystallographically independent structural units, as the BDS^{2-} dianion contains an inversion centre (Fig. S2). Electrostatic N–H$^+$•••$^-$O$_3$S– hydrogen bonds tightly connect the G^+ cations and BDS^{2-} anions, forming a one-dimensional (1D) chain of $[(G^+)^2(BDS^{2-})]_\infty$ along the *b*+*c* axes with N•••O distances d_{N-O}=2.963(3) and 2.902(3) Å (white dashed lines in Fig. 1a).

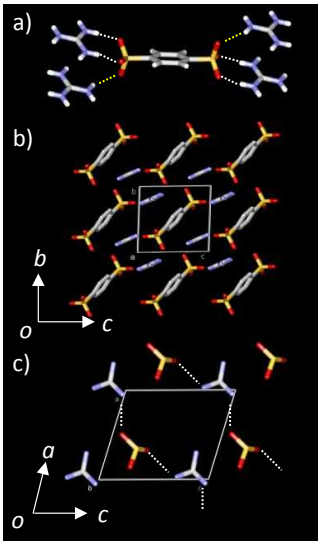

Fig. 1. Crystal structure of guest-free $(G^+)_2(BDS^{2-})$ at 100 K. a) Tightly bound ions by double electrostatic N–H$^+$•••$^-$O$_3$S– hydrogen bonds. b) Unit cell viewed along *a* axis. c) Hydrogen bonds on the *ac* plane.

This 1D chain is further stabilized by an additional N–H$^+$•••$^-$O$_3$S– hydrogen bond with d_{N-O}=3.026(3) Å (yellow dashed line in Fig. 1a). Fig. 1b shows the unit cell viewed along the *a* axis. The G^+ dimers and BDS^{2-} dianions are arranged alternately in the *bc* plane and linked by electrostatic hydrogen bonds (Fig. S3). Furthermore, the 1D chains of $[(G^+)^2(BDS^{2-})]_\infty$ interact along both the *a* and *c* axes (Fig. 1c), forming a three-dimensional (3D) hydrogen bonding network with d_{N-O}=2.915(3) and 2.974(2) Å along the *a* and *c* axes, respectively. The electrostatically bound cation–dianion $(G^+)_2(BDS^{2-})$ crystal lattice is dynamically responsive to guest adsorption by the modulation of the 3D hydrogen bonding network.

Crystal structures of $(G^+)_2(BDS^{2-})\bullet(H_2O$ or Pyz).

Fig. 2 summarises the crystal structure of $(G^+)_2(BDS^{2-})\bullet(H_2O)$ at 100 K. Two G^+ cation and one BDS^{2-} dianion are the crystallographically independent structural units (Fig. S4). Two orientations with an equal occupation factor were observed in phenyl-ring of BDS^{2-} dianion (grey and blue structures in Fig. 2a). The electrostatic N–H$^+$•••$^-$O$_3$S– hydrogen-bonding lattice of $(G^+)_2$•••BDS^{2-} formed the 2D layer in the *bc* plane (Fig. 2b and Fig. S5), where the guest H_2O molecules existed in the cylindrical space surrounded by the four phenyl-rings of BDS^{2-} and two capped G^+ cations at the upper and lower space of the cylinder. The 2D cylinder array in the *bc* plane was stacked along the *a* axis, forming the bilayer structure of the 2D electrostatic N–H$^+$•••$^-$O$_3$S– hydrogen-bonding layer (Fig. 2b). Effective hydrogen-bonding interactions of d_{N-O} = 2.987(7) and 2.987(8) Å (white dashed lines in Fig. 2c) formed the tight electrostatic G^+•••BDS^{2-} pairs, which were further connected by the additional hydrogen-bonding interactions of d_{N-O} = 2.996(7) and 2.932(7) Å in the *bc* plane (yellow dashed lines in Fig. 2c). The guest H_2O molecule existed in the cylindrical cavity space without the effective hydrogen-bonding interaction.

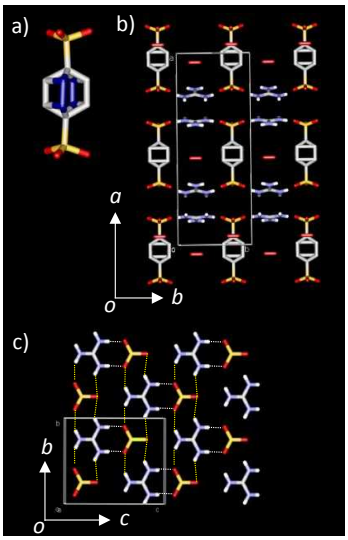

Fig. 2. Crystal structure of $(G^+)_2(BDS^{2-})\bullet(H_2O)$ at 100 K. a) Orientational disorder of phenyl-ring of BDS^{2-} dianion. b) Unit cell viewed along *a* axis. c) Hydrogen bonds on the *bc* plane.

Fig. 3 shows the crystal structure of $(G^+)_2(BDS^{2-})\bullet$(Pyz) at 100 K. One G^+ cation, a half unit of BDS^{2-} dianion and Pyz were the crystallographically independent structural units, as the BDS^{2-} dianion contains an inversion centre (Fig. S6). The packing structure of $(G^+)_2(BDS^{2-})\bullet$(Pyz) was similar to that of $(G^+)_2(BDS^{2-})\bullet(H_2O)$. The 2D electrostatic N–H$^+$•••$^-$O$_3$S– hydrogen-bonding layer existed in the *ab* plane, and guest Pyz

molecule was sandwiched by two phenyl-rings of $\mathbf{BDS^{2-}}$ dianions along the *b* axis (Figs. 3a and 3b). The effective hydrogen-bonding interactions of $d_{N\text{-}O}$ = 2.913(9) and 2.939(3) Å (white dashed lines in Fig. 3c) formed the tight electrostatic $\mathbf{G^{+}}$•••$\mathbf{BDS^{2-}}$ pairs, which were further interacted by the additional hydrogen-bonding interaction of $d_{N\text{-}O}$ = 2.950(3) Å in the *ab* plane (yellow dashed lines in Fig. 3c). The guest Pyz molecule formed the alternate π-stacking column of •••$\mathbf{BDS^{2-}}$•••Pyz•••$\mathbf{BDS^{2-}}$••• along the *b* axis, where the average π-plane of Pyz was 7.2 ° inclined to the π-plane of $\mathbf{BDS^{2-}}$ dianion (Fig. 3d and Fig. S7). Although the magnitude of V_G = 60 Å^3 for Pyz was 6 times larger than that of V_G = 10 Å^3 for H_2O, similar bilayer type electrostatic $(\mathbf{G^{+}})_2$•••$\mathbf{BDS^{2-}}$ hydrogen-bonding layers were observed in the *bc* and *ab* planes, respectively.

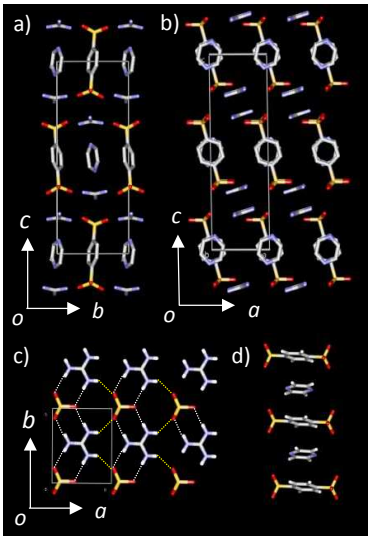

Fig. 3. Crystal structure of $(\mathbf{G^{+}})_2(\mathbf{BDS^{2-}})$•(Pyz) at 100 K. Unit cell viewed a) along the *a* axis and b) along the *b* axis. c) Hydrogen-bonding layer on the *bc* plane. d) Alternate π-stacking column of $\mathbf{BDS^{2-}}$ and Pyz.

Crystal structure of $(\mathbf{G^{+}})_2(\mathbf{BDS^{2-}})$•$(\mathbf{Py\text{-}H_2O})_2$.

The crystal structure of $(\mathbf{G^{+}})_2(\mathbf{BDS^{2-}})$•$(\text{Py-H}_2\text{O})_2$ at 100 K resembles that of $(\mathbf{G^{+}})_2(\mathbf{BDS^{2-}})$•$(\text{THF})_2$ in previous,[47] and both are different from that of the previously discussed 1:1 stoichiometric $(\mathbf{G^{+}})_2(\mathbf{BDS^{2-}})$•($H_2O$ or Pyz) crystals. The guest molecules THF and Py have V_G of 71 and 65 Å^3, respectively. The crystal structure of $(\mathbf{G^{+}})_2(\mathbf{BDS^{2-}})$•$(\text{Py-H}_2\text{O})_2$ resembles that of $(\mathbf{G^{+}})_2(\mathbf{BDS^{2-}})$•$(\text{THF})_2$ with an electrostatic hydrogen-bonded bilayer structure on the *bc* plane, whereas the pillared $\mathbf{BDS^{2-}}$ dianions are found along the *a* axis (Fig. 4). One $\mathbf{G^{+}}$ cation, a half unit of $\mathbf{BDS^{2-}}$ dianion, and one Py are the crystallographically independent structural units, as the $\mathbf{BDS^{2-}}$ dianion contains an inversion centre (Fig. S11). The 1D guest-capturing channels along the *b* axis, in the absence of the void space along the *a* axis, are occupied by the guest Py molecules. Additionally, 2 H_2O molecules are sandwiched between the hydrogen-bonded 2D layers, forming the small pillared hydrogen-bonded assembly $(\mathbf{G^{+}})_2(\mathbf{BDS^{2-}})$•••$(H_2O)_2$•••$(\mathbf{G^{+}})_2(\mathbf{BDS^{2-}})$ on the *bc* plane (Figs S12 and S14). The 1D hydrogen-bonded zig-zag chain of $[(\mathbf{G^{+}})(\mathbf{BDS^{2-}})]_\infty$ along the *b* axis has $d_{N\text{-}O}$ = 2.880(2), 2.970(2), 2.904(2), and 2.956(2) Å, and these chains are connected along the *c* axis by additional H_2O molecules through two N–H$^+$•••O– interactions ($d_{N\text{-}O}$= 2.885(2) and 2.931(2) Å) and one $-SO_3^-$•••H–O interaction ($d_{O\text{-}O}$=2.843(2) Å). The bilayer structure is constructed by electrostatic hydrogen bonds through the H_2O molecules. A structural reconstruction to the 1D hydrogen-bonded zig-zag chain containing additional H_2O molecules occurs upon adsorption of Py and H_2O molecules in the $(\mathbf{G^{+}})(\mathbf{BDS^{2-}})$ host lattice (Fig. S13).

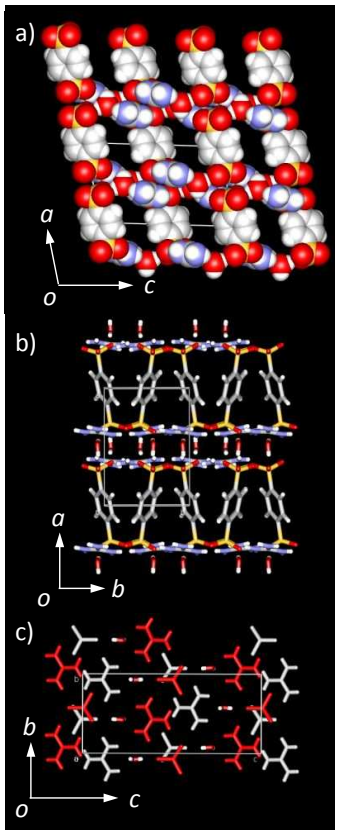

Fig. 4. Crystal structure of $(\mathbf{G^{+}})_2(\mathbf{BDS^{2-}})$•$(\text{Py-H}_2\text{O})_2$ at 100 K. Unit cells viewed a) along the *b* axis (CPK representation) and b) along the *c* axis. The guest molecules are omitted for clarity. c) The 2D hydrogen-bonded bilayer structure on the *bc* plane. Red and grey denote molecules in the upper and lower layers, respectively.

Crystal structure of $(\mathbf{G^{+}})_2(\mathbf{BDS^{2-}})$•(Diox, Ani, TP, or Pyrr)$_3$.

Single-crystals of 1:3 stoichiometric $(\mathbf{G^{+}})_2(\mathbf{BDS^{2-}})$•$(\text{Benz})_3$, $(\mathbf{G^{+}})_2(\mathbf{BDS^{2-}})$•$(\text{Diox})_3$, $(\mathbf{G^{+}})_2(\mathbf{BDS^{2-}})$•$(\text{Ani})_3$, $(\mathbf{G^{+}})_2(\mathbf{BDS^{2-}})$•$(\text{TP})_3$, and $(\mathbf{G^{+}})_2(\mathbf{BDS^{2-}})$•$(\text{Pyrr})_3$ are isostructural at 100 K. In these crystals, the guest molecule V_G increased in the order of Pyrr (56 Å^3), TP (61 Å^3), Benz (71 Å^3), Diox (78 Å^3), to Ani (80 Å^3). One $\mathbf{G^{+}}$ cation, a half unit of $\mathbf{BDS^{2-}}$, and one and half units of Benz (Fig. S15), Diox (Figs S16-S19), TP (Figs S20-S22), and Pyrr (Figs S23-S25) are the crystallographically independent structural units. Interestingly, non-centrosymmetrical space group of $P2_1$ was observed in single crystals of $(\mathbf{G^{+}})_2(\mathbf{BDS^{2-}})$•(Ani), where the crystal symmetrical was converted from a centric *P*-1 in the host $(\mathbf{G^{+}})_2(\mathbf{BDS^{2-}})$ framework to acentric $P2_1$ after Ani adsorption (Fig. S26). The molecular structures of guest molecules for Diox and Ani could be determined in the single-crystal X-ray structural analyses at 100 K, whereas the small guest molecules of Pyrr and TP were difficult to determine the molecular structures and

orientation. In Figs 5a and 5b, the unit cells are displayed along the *a* and *b* axes (Fig. S16), respectively, and the void spaces are visible in the CPK representation (the guest molecules are omitted for clarity). Large void spaces for the adsorption of guest Diox molecules exist in the *bc* and *ac* planes. In the *ab* plane (Fig. 5c), a network of N–H$^+$•••$^-$O$_3$S– hydrogen bonds tightly connected **G**$^+$ and **BDS**$^{2-}$ with six different $d_{N\text{-}O}$ distances (2.902(7), 2.888(7), 2.862(7), 2.947(7), 2.985(7), and 2.873(7) Å). Between the nearly planar 2D hydrogen bonding layers, which extend on the *ab* plane, the **BDS**$^{2-}$ dianions form a pillared pore structure. Upon guest adsorption, guest-free (**G**$^+$)$_2$(**BDS**$^{2-}$) undergoes a structural reconstruction to the host–guest pillared supramolecular structure. The guest Diox molecules occupy the pores, forming a herringbone arrangement along the *a* axis, whereas the 1D Diox array elongates along the *b* axis (Fig. 5d). On the *ab* plane there are 2D crystalline spaces between the pillars, and herringbone and π-stacking interactions exist along the *a* and *b* axes, respectively.

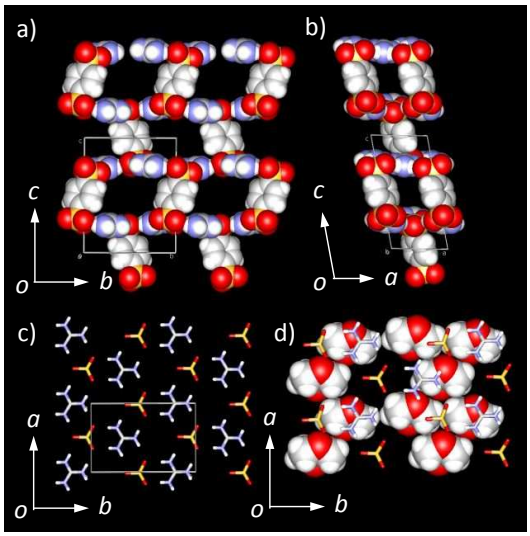

Fig. 5. Crystal structure of (**G**$^+$)$_2$(**BDS**$^{2-}$)•(Diox)$_3$ at 100 K. Unit cells viewed a) along the *a* axis and b) along the *b* axis. CPK representation was used, and the guest Diox molecules are omitted for clarity. c) The 2D electrostatic hydrogen-bonded layer on the *ab* plane viewed along the *c* axis. d) Packing structure of the Diox guest molecules on the *ab* plane.

Adsorption–desorption isotherms.

The (**G**$^+$)$_2$(**BDS**$^{2-}$) host lattice is tightly connected by electrostatic hydrogen bonds, and does not contain void spaces. Guest adsorption in the host lattice led to a structural reconstruction, generating a large volume of void space. Figs. 6a and 6b show the adsorption–desorption isotherms of guest-free (**G**$^+$)$_2$(**BDS**$^{2-}$) crystals for THF and Diox at 288 and 298 K, respectively. The THF adsorption–desorption isotherm of the crystalline (**G**$^+$)$_2$(**BDS**$^{2-}$) powder indicated reversible gate-opened adsorption–desorption behaviour. The maximum adsorption amount (n_{max}) of THF molecules per (**G**$^+$)$_2$(**BDS**$^{2-}$) of n_{max}=3.5 with P/P_0=1.0 is inconsistent with the results of single-crystal X-ray structural analysis at 100 K. When the relative pressure of P/P_0 was increased to P/P_0=0.6, a sudden increase in the n_{ad} was observed, and saturation was reached at n_{max}=3.5 with P/P_0=1.0. Regarding the desorption process, the crystalline (**G**$^+$)$_2$(**BDS**$^{2-}$)•(THF)$_{3.5}$ powder was stable as the relative pressure was reduced until P/P_0=0.3. The bilayer-type hydrogen-bonded network exists in the crystal structure of (**G**$^+$)$_2$(**BDS**$^{2-}$)•(THF)$_2$,[47] and the intra-layer features electrostatic interactions. Additional 1.5 THF molecules were inserted into the intra-layer space of (**G**$^+$)$_2$(**BDS**$^{2-}$)•(THF)$_2$ to form the (**G**$^+$)$_2$(**BDS**$^{2-}$)•(THF)$_{3.5}$ crystals.

Almost the same gate-opened adsorption–desorption isotherm was observed with Diox, and single-crystal X-ray analysis indicated the formula (**G**$^+$)$_2$(**BDS**$^{2-}$)•(Diox)$_3$. In the adsorption cycle, a sudden n_{ad} enhancement was also observed at P/P_0=0.6, and the reached n_{ad}=3.0 corresponds to an ideal crystal formula of (**G**$^+$)$_2$(**BDS**$^{2-}$)•(Diox)$_3$. In the desorption cycle, the host–guest crystal formula of (**G**$^+$)$_2$(**BDS**$^{2-}$)•(Diox)$_3$ was stable until P/P_0=0.1, and a sudden desorption to n_{ad}=0 occurred upon further decrease in the relative pressure. The hydrogen-bonded simple brick structure of (**G**$^+$)$_2$(**BDS**$^{2-}$)•(Diox)$_3$ did not have additional adsorption pores for Diox. Therefore, the host (**G**$^+$)$_2$(**BDS**$^{2-}$) crystal lattice was consistent with a maximum n_{ad}=3.0 for Diox adsorption.

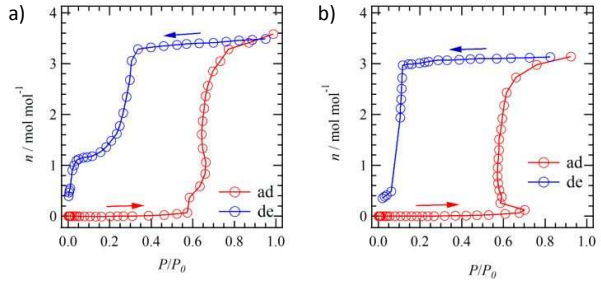

Fig. 6. The adsorption–desorption isotherms of the host (**G**$^+$)$_2$(**BDS**$^{2-}$) crystals for a) THF at 288 K and b) Diox at 289 K. Adsorption and desorption are abbreviated ad and de, respectively.

Figs. 7a and 7b present the changes in the PXRD patterns of the crystals (**G**$^+$)$_2$(**BDS**$^{2-}$)•(THF)$_3$ and (**G**$^+$)$_2$(**BDS**$^{2-}$)•(Diox)$_2$ during the guest adsorption–desorption cycles. According to the TG analyses of (**G**$^+$)$_2$(**BDS**$^{-2}$)•(Guest)$_x$ crystals, guest desorption begins at 300 K. The PXRD pattern of host–guest crystals of (**G**$^+$)$_2$(**BDS**$^{2-}$)•(THF)$_3$ at 298 K differs slightly from the simulated one because of the THF desorption process (Fig. 7a, i and ii). In contrast, the PXRD pattern of the (**G**$^+$)$_2$(**BDS**$^{2-}$)•(Diox)$_2$ crystals at 298 K was consistent with the simulated one (Fig. 7b, i and ii), suggesting that the crystal containing Diox molecules is more stable than the one containing THF molecules in the pore spaces. The guest molecules were completely removed by thermal treatment of the host–guest crystals (**G**$^+$)$_2$(**BDS**$^{2-}$)•(Guest)$_x$ at 473 K, forming guest-free (**G**$^+$)$_2$(**BDS**$^{2-}$) crystals. The PXRD patterns of the latter were consistent with the simulated one (Figs. 7a and 7b, iii and iv). High crystallinity was observed in the PXRD patterns of guest-free (**G**$^+$)$_2$(**BDS**$^{2-}$) crystals after the thermal treatment. Therefore, the guest adsorption–desorption cycles were the outer triggers of the dynamic structural reconstruction between (**G**$^+$)$_2$(**BDS**$^{2-}$)•(Guest)$_x$ and (**G**$^+$)$_2$(**BDS**$^{2-}$). The tightly bound electrostatic crystal lattice of (**G**$^+$)$_2$(**BDS**$^{2-}$) is useful for dynamic structural reconstruction, while maintaining high crystallinity. In addition, the changes of temperature and time dependent

PXRD patterns of $(G^+)_2(BDS^{2-})\bullet(THF)_2$ were evaluated in the single crystalline state (Fig. S30), which clearly indicated the structural reconstruction from $(G^+)_2(BDS^{2-})\bullet(THF)_2$ to $(G^+)_2(BDS^{2-})$ by increasing in the temperatures. This structural reconstruction occurred in the highly crystalline state.

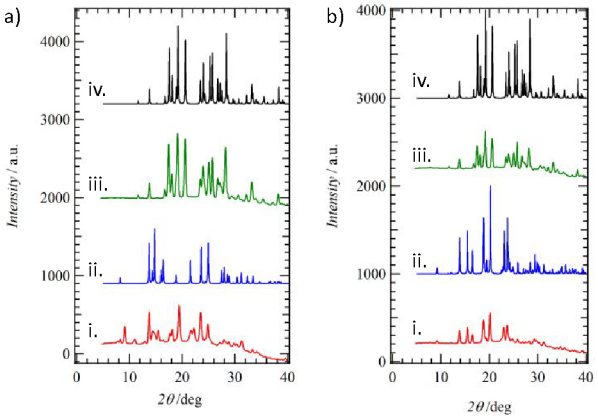

Fig. 7. PXRD patterns of guest adsorption–desorption cycle of the host $(G^+)_2(BDS^{2-})$ crystals for a) THF and b) Diox molecules. i) Simulated pattern of $(G^+)_2(BDS^{2-})\bullet(Guest)_x$ crystals based on single-crystal X-ray structural analysis at 100 K, ii) PXRD pattern of $(G^+)_2(BDS^{2-})\bullet(Guest)_x$ crystals at 298 K, iii) PXRD pattern of $(G^+)_2(BDS^{2-})$ crystals after the removal of guest molecules by thermal treatment, and iv) simulated pattern of $(G^+)_2(BDS^{2-})$ crystals based on the single-crystal X-ray structural analysis at 100 K.

Mechanism of structural reconstruction.

The host crystal lattice of $(G^+)_2(BDS^{2-})$ is held together by charge supported hydrogen bonds and does not contain void spaces. Scheme 2 summarises the dynamic lattice reconstruction from the guest-free $(G^+)_2(BDS^{2-})$ to the guest-capturing $(G^+)_2(BDS^{2-})\bullet(Guest)_x$ for H_2O, Benz, Ani, Diox, THF, Pyz, Py, TP, and Pyrr based on the single-crystal X-ray structural analyses at 100 K and the adsorption–desorption isotherms of THF and Diox. The adsorption of Benz, Ani, Diox, TP, and Pyrr transformed the host crystal lattice to a pillared host–guest framework, forming 1:3 stoichiometric $(G^+)_2(BDS^{2-})\bullet(Guest)_3$ crystals in which the electrostatic N–H•••$^-$O$_3$S– hydrogen-bonded simple brick and pillared BDS^{2-} dianions generated the guest adsorption pores between the pillars. Interestingly, the molecular arrangement of guest Ani molecules in $(G^+)_2(BDS^{2-})\bullet(Ani)_3$ single-crystal was non-centrosymmetrical arranged (Fig. S29), suggesting the symmetry lowering of the host framework by guest Ani adsorption. In contrast, adsorption of THF and Py led to $(G^+)_2(BDS^{2-})\bullet$(THF or Py-$H_2O)_2$ crystals featuring a pillared host–guest framework with a hydrogen-bonded bilayer. The inclusion of H_2O molecules concomitant with the Py adsorption results in the hydrogen-bonded bilayer structure $[(G^+)_2(BDS^{2-})\bullet\bullet\bullet(H_2O)_2\bullet\bullet\bullet(G^+)_2(BDS^{2-})]$. The additional 1.5 THF molecules in the $(G^+)_2(BDS^{2-})\bullet(THF)_{3.5}$ crystal suggested the formation of a $[(G^+)_2(BDS^{2-})\bullet\bullet\bullet(THF)_{1.5}\bullet\bullet\bullet(G^+)_2(BDS^{2-})]$ intra-layer in addition to the inclusion of 2 THF in the inter-layer. In contrast, the tight binding of the hydrogen-bonded bilayer in the $(G^+)_2(BDS^{2-})\bullet$(Py-$H_2O)_2$ crystals suppressed the elimination of H_2O and replaced the additional Py molecules into the bilayer space. The flexible and dynamic $(G^+)_2(BDS^{2-})$ host lattice was able to adsorb various guest molecules, forming different types of host–guest molecular crystals. The adsorption of H_2O and **Pyz** led to $(G^+)_2(BDS^{2-})\bullet$(H_2O or Pyz) crystals featuring a pillared host–guest framework with a hydrogen-bonded bilayer. The π-stacking alternate columnar structure of •••Pyz•••BDS^{2-}•••Pyz••• was observed in the 2D layer, while the H_2O molecules were loosely kept in the cage surrounded by the four phenyl-rings of BDS^{2-} and two capping G^+ cations. According to the guest molecules, three kinds of host–guest stoichiometries of $(G^+)_2(BDS^{2-})\bullet(Guest)_x$ (x = 1, 2, and 3) were observed in the single-crystal X-ray structural analyses at 100 K.

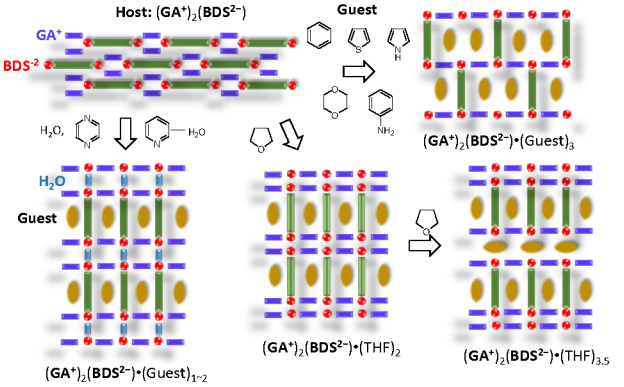

Scheme 2. Dynamic structural reconstruction of the guest-free $(G^+)_2(BDS^{2-})$ framework upon adsorption of H_2O, Benz, Pyz, Diox, THF, Py, Ani, TP, and Pyrr. The G^+, BDS^{2-}, H_2O, and guest molecules are represented by violet, green-red, blue, and brown objects, respectively.

Conclusions

The electrostatically bound cation–anion host framework of $(G^+)_2(BDS^{2-})$ underwent a dynamic structural reconstruction upon reversible introduction of H_2O (V_G = 10 Å^3), Pyrr (V_G = 56 Å^3), Pyz (V_G = 60 Å^3), TP (V_G = 61 Å^3), Py (V_G = 65 Å^3), THF (V_G = 71 Å^3), Benz (V_G = 71 Å^3), Diox (V_G = 78 Å^3), and Ani (V_G = 80 Å^3) into the host–guest single crystals within the guest adsorption–desorption cycle. Cationic G^+ and dianionic BDS^{2-} formed a 2D electrostatic N–H$^+$•••$^-$O$_3$S– hydrogen-bonded layer, whereas the BDS^{2-} molecules acted as dynamic pillars to generate the guest adsorption crystalline pores. The hydrogen-bonded $[(G^+)_2(BDS^{2-})]$ bricks and $[(G^+)_2(BDS^{2-})]_2$ bilayers were observed in the single-crystal X-ray structural analyses of $(G^+)_2(BDS^{2-})\bullet$(Pyrr, TP, Py, Benz, Diox or Ani)$_3$, $(G^+)_2(BDS^{2-})\bullet$(THF or Py-$H_2O)_2$, and $(G^+)_2(BDS^{2-})\bullet$(H_2O or Pyz), respectively. The guest adsorption crystalline spaces in the bilayer-type crystals were smaller than those in the brick ones. However, the bilayer-type $[(G^+)_2(BDS^{2-})]_2$ enabled intra-layer THF adsorption to form $(G^+)_2(BDS^{2-})\bullet(THF)_{3.5}$, as revealed by the corresponding adsorption–desorption isotherm at 288 K. The crystal structure of $(G^+)_2(BDS^{2-})\bullet$(Py-$H_2O)_2$ features H_2O linkers between the $(G^+)_2(BDS^{2-})$ bricks, forming the bilayer $[(G^+)_2(BDS^{2-})\bullet\bullet\bullet(H_2O)_2\bullet\bullet\bullet(G^+)_2(BDS^{2-})]$. The adsorption–desorption isotherms for Diox and THF indicated reversible gate-opened molecular sorption properties. The structurally rigid and adaptable cation–anion electrostatic framework of $(G^+)_2(BDS^{2-})$ underwent a dynamic structural reconstruction from guest-free non-porous ionic crystals to the pillar-standing guest adsorption crystals. Dynamic molecular assemblies based

on electrostatic interactions are interesting materials with high thermal and chemical stability that are responsive to outer stimuli.

Conflicts of interest

There are no conflicts to declare.

Acknowledgements

This work was supported by a Grant-in-Aid for Scientific Research on KAKENHI Kibankenkyu (A) (JP19H00886), JST CREST (Grant Number JPMJCR18I4), the "Network Joint Research Center for Materials and Devices", and the "Dynamic Alliance for Open Innovation Bridging Human, Environment and Materials" project supported by MEXT.

Notes and references

1 A. I. Kitaigorodsky, *Molecular Crystals and Molecules*. Academic Press, New York, 1973.
2 F. H. Herbstein, *Crystalline Molecular Complexes and Compounds: Structures and Principles*, Oxford Scientific Publication, 2005.
3 J. D. Dunitz, A. Gavezzotti, *Chem. Soc. Rev*. **2009**, *38*, 2622–2633.
4 A. Gavezzotti, *Molecular Aggregation: Structure analysis and molecular simulation of crystals and liquids*, Oxford Scientific Publication, 2010.
5 K. Goossens, K. Lava, C. W. Bielawski, K. Binnemans, *Chem. Rev*. **2016**, *116*, 4643–4807.
6 J. M. Pringle, P. C. Howlett, D. R. MacFarlane, M. Forsyth, *J. Mater. Chem*. **2010**, *20*, 2056–2062.
7 J. Harada, T. Shimojo, H. Oyamaguchi, H. Hasegawa, Y. Takahashi, K. Satomi, Y. Suzuki, J. Kawamata, T. Inabe, *Nat. Chem*. **2016**, *8*, 946–952.
8 D. –W. Fu, H.-L. Cai, Y. Liu, Q. Ye, W. Zhang, Y. Zhang, X.-Y. Chen, G. Giovannetti, M. Capone, J. Li, R.-G. Xiong, *Science* **2013**, *339*, 425–428.
9 D.-W. Fu, W. Zhang, H.-L. Cai, J. -Z. Ge, Y. Zhang, R.-G. Xiong*Adv. Mater*. **2011**, *23*, 5658–5662.
10 M. Szafranski, J. Wolak, M. Połomska, *J. Phys. Chem. C* **2018**, *122*, 22054−22062.
11 J. Wu, T. Takeda, N. Hoshino, Y. Suzuki, J. Kawamata, T. Akutagawa, *J. Phys. Chem. C* **2019**, *123*, 22439–22446.
12 A. Kawasaki, T. Takeda, N. Hoshino, W. Matsuda, S. Seki, T. Akutagawa, *J. Phys. Chem. C* **2019**, *123*, 15451–15457.
13 A. Kawasaki, T. Takeda, N. Hoshino, W. Matsuda, S. Seki, T. Akutagawa, *Cryst. Growth Des*. **2020**, *20*, 1276–1284.
14 C. F. C. Faul, *Acc. Chem. Res*. **2014**, *47*, 3428−3438.
15 D. Wu, R. Liu, W. Pisula, X. Feng, K. Müllen, *Angew. Chem. Int. Ed*. **2011**, *50*, 2791–2794.
16 T. Sakai, S. Seo, J. Matsuoka, Y. Mori, *J. Org. Chem*. **2013**, *78*, 10978−10985.
17 H. Maeda, Y. Haketa, T. Nakanishi, *J. Am. Chem. Soc*. **2007**, *129*, 13661−13674.
18 T. Yuge, I. Hisaki, M. Miyata, N. Tohnai, *CrystEngComm*. **2008**, *10*, 263−266.
19 J. Tian, T. –Y. Zhou, S. -C. Zhang, S. Aloni, M. V. Altoe, S. -H. Xie, H. Wang, D. –W. Zhang, X. Zhao, Y. Liu, X. –T. Li, *Nat. Commun*. **2014**, *5*, 5574-1-11.
20 A. Yamamoto, S. Uehara, T. Hamada, M. Miyata, I. Hisaki, N. Tohnai, *Cryst. Growth Des*. **2012**, *12*, 4600–4606.
21 G. K. H. Shimizu, R. Vaidhyanathan, J. M. Taylor, *Chem. Soc. Rev*. **2009**, 38, 1430–1449.
22 I. Hisaki, *J. Incl. Phenom. Macrocycl. Chem*. **2020**, *96*, 215–231.
23 P. J. Waller, F. Gándara, O. M. Yaghi, *Acc. Chem. Res*. **2015**, *48*, 3053–3063.
24 W. Yang, A. Greenaway, X. Lin, R. Matsuda, A. J. Blake, C. Wilson, W. Lewis, P. Hubberstey, S. Kitagawa, N. R. Champness, M. Schröder, *J. Am. Chem. Soc*. **2010**, *132*, 14457–14469.
25 J. Luo, J. –W. Wang, J. -H. Zhang, S. Lai, D. –C. Zhong, *CrystEngComm*. **2018**, *20*, 5884–5898.
26 Y. He, S. Xiang, B. A. Chen, *J. Am. Chem. Soc*. **2011**, *133*, 14570−14573.
27 A. Pulido, L. Chen, T. Kaczorowski, D. Holden, M. A. Little, S. Y. Chong, B. Slater, D. P. McMahon, B. Bonillo, C. Stackhouse, A. Stephenson. C. M. Kane, R. Clowes, T. Hasell, A. I. Cooper, *Nature* **2017**, *543*, 657–666.
28 P. Cui, D. P. McMahon, R. P. Spackman, B. M. Alston, M. A. Little, G. M. Day, A. I. Cooper, *Chem. Sci*. **2019**, *10*, 9988–9997.
29 I. Hisaki, S. Nakagawa, M. Tohnai, M. A. Miyata, *Angew. Chem. Int. Ed*. **2015**, *54*, 3008–3012.
30 S. Uchikawa, A. Kawasaki, N. Hoshino, T. Takeda, K. Takahasi, S. Noro, T. Nakamura, N. Sato, K. Kokubo, H. Sakurai, T. Akutagawa, *J. Phys. Chem. C*, **2019**, *123*, 23544−23553.
31 T. Takeda, M. Ozawa, T. Akutagawa, *Angew. Chem. Int. Ed*. **2019**, *58*, 10345–10352.
32 G. Yuan, T. Takeda, N. Hoshino, T. Akutagawa, *Cryst. Growth Des*. **2019**, *19*, 3509−3517.
33 G. A. Jeffrey, *An Introduction to Hydrogen Bonding*. Truhlar, D. G.; Ed.; Oxford University Press: New York, 1997.
34 L. J. Prins, D. N. Reinhoudt, P. Timmerman, *Angew. Chem. Int. Ed.* **2001**, *40*, 2382−2426.
35 T. Akutagawa, *Mater. Chem. Front*. **2018**, *2*, 1064–1073.
36 M. K. Corpino, D. -K.; Bučar, *Cryst. Growth Des*. **2019**, *19*, 1426−1453.
37 V. A. Russell, C. C. Evans, W. Li, M. D. Ward, *Science* **1997**, *276*, 575–579.
38 T. Adachi, M. D. Ward, *Acc. Chem. Res*. **2016**, *49*, 2669–2679.
39 K. T. Holman, A. M. Pivovar, J. A. Swift, M. D. Ward, *Acc. Chem. Res*. **2001**, *34*, 107–108.
40 K. T. Holman, A. M. Pivovar, M. D. Ward, *Science* **2001**, *294*, 1907–1911.
41 W. Xiao, C. Hu, M. D. Ward, *J. Am. Chem. Soc*. **2014**, *136*, 14200–14206.
42 D. J. Plaut, K. T. Holman, A. M. Pivovar, M. D. Ward, *J. Phys. Org. Chem*. **2000**, *13*, 858–869.
43 A. N. Holden, W. J. Merz, J. P. Remeika, B. T. Matthias, *Phys. Rev*. **1956**, *101*, 962−966.
44 M. Szafrański, M. Jarek, *J. Phys. Chem. B* **2008**, *112*, 3101−3109.
45 F. Mathevet, P. Masson, J. –P. Nicoud, A. Skoulios, *J. Am. Chem. Soc*. **2005**, *127*, 9053−9061.
46 V. A. Russell, M. C. Etter, M. D. Ward, *Chem. Mater*. **1994**, *6*, 1206−1217.
47 K. T. Holman, S. M. Martin, D. P. Parker, M. D. Ward, *J. Am. Chem. Soc*. **2001**, *123*, 4421−4431
48 K. T. Holman, M. D. Ward, *Angew. Chem. Int. Ed*. **2000**, *39*, 1653−1655
49 I. Brekalo, D. E. Deliz, L. J. Barbour, M. D. Ward, T. Friščić, K. T. Holman. *Angew. Chem. Int. Ed*. **2020**, *59*, 1997−2002
50 W. Xiao, C. Hu, M. D. Ward, *J. Am. Chem. Soc*. **2014**, *136*, 14200−14206
51 Y. Li, M. Handke, Y. –S. Chen, A. G. Shtukenberg, C. T. Hu, M. D. Ward, *J. Am. Chem. Soc*. **2018**, *140*, 12915−12921.
52 A. Karmakar, R. Illathvalappil, B. Anothumakkool, A. Sen, P. Samanta, A. V. Desai, S. Kurungot, S. K. Ghosh, *Angew. Chem. Int. Ed*. **2016**, *128*, 10825–10829.

53 Y. Li, S. Tang, A. Yusov, J. Rose, A. N. Borrfors, C. T. Hu, M. D. Ward, *Nature Comm*. **2019**, *10*, 4477-1-7.
54 M. L. Connolly, *J. Am. Chem. Soc*. **1985**, *107*, 1118–1124.
55 Crystal Structure: Single Crystal Structure Analysis Software. Ver. 3.6, **2010**. Rigaku Corporation and Molecular Structure Corporation.
56 Sheldrick, G. M. SHELXL Version 2018 *Programs for Crystal Structure Analysis*; Universitat Göttingen: Göttingen, Germany, **1998**.

TOC

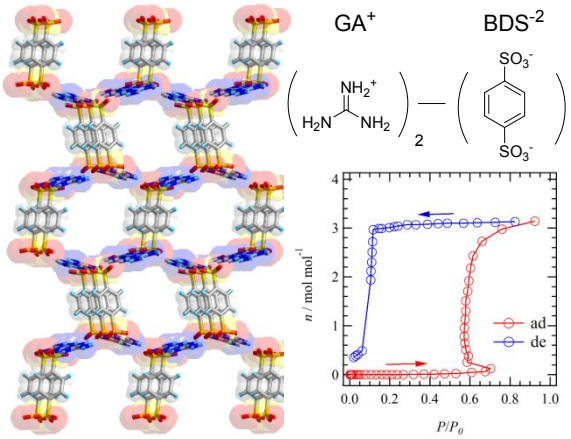
GA+
BDS-2
NH2+
H2N
NH2
2
SO3-
SO3-
n / mol mol-1
ad
de
P/P0
0.0
0.2
0.4
0.6
0.8
1.0
0
1
2
3
4